MOLECULAR AND CELLULAR BIOLOGY, Apr. 2007, p. 2870–2885 Vol. 27, No. 8
0270-7306/07/$08.00+0 doi:10.1128/MCB.02323-06

A Modular Enhancer Is Differentially Regulated by GATA and NFAT Elements That Direct Different Tissue-Specific Patterns of Nucleosome Positioning and Inducible Chromatin Remodeling▽

Andrew G. Bert,[1]† Brett V. Johnson,[2]†‡ Euan W. Baxter,[2] and Peter N. Cockerill[2]*

Hanson Institute, Institute of Medical and Veterinary Science, Adelaide 5000, Australia,[1] and Experimental Haematology, Leeds Institute of Molecular Medicine, St. James's University Hospital, Leeds LS9 7TF, United Kingdom[2]

Received 12 December 2006/Returned for modification 24 January 2007/Accepted 27 January 2007

We investigated alternate mechanisms employed by enhancers to position and remodel nucleosomes and activate tissue-specific genes in divergent cell types. We demonstrated that the granulocyte-macrophage colony-stimulating factor (GM-CSF) gene enhancer is modular and recruits different sets of transcription factors in T cells and myeloid cells. The enhancer recruited distinct inducible tissue-specific enhanceosome-like complexes and directed nucleosomes to different positions in these cell types. In undifferentiated T cells, the enhancer was activated by inducible binding of two NFAT/AP-1 complexes which disrupted two specifically positioned nucleosomes (N1 and N2). In myeloid cells, the enhancer was remodeled by GATA factors which constitutively displaced an upstream nucleosome (N0) and cooperated with inducible AP-1 elements to activate transcription. In mast cells, which express both GATA-2 and NFAT, these two pathways combined to activate the enhancer and generate high-level gene expression. At least 5 kb of the GM-CSF locus was organized as an array of nucleosomes with fixed positions, but the enhancer adopted different nucleosome positions in T cells and mast cells. Furthermore, nucleosomes located between the enhancer and promoter were mobilized upon activation in an enhancer-dependent manner. These studies reveal that distinct tissue-specific mechanisms can be used either alternately or in combination to activate the same enhancer.

The complex patterns of gene expression found within diverse cell types are tightly controlled by a wide variety of tissue-specific and inducible transcription factors that have overlapping expression patterns. The aims of the studies presented here are to determine (i) whether genes recruit the same or alternate sets of transcription factors in the different cell types in which a specific gene is expressed, (ii) whether transcription factor recruitment alters nucleosome positioning, and (iii) whether nucleosomes adopt the same or different positions when controlled by different sets of transcription factors. Surprisingly few studies, if any at all, have addressed the latter questions, in particular in the context of natural gene loci in higher eukaryotes.

There is also considerable evidence that the context of transcription factor binding sites is crucial to their function, with arrays of specifically positioned elements assembling multiprotein complexes termed enhanceosomes (5, 8, 28, 29). Enhanceosomes are likely to assemble at sites of protein-protein interactions on DNA, such as those that join NFAT and AP-1 at composite elements (8), and can assemble using coactivators such as CBP and P300 as scaffolding proteins (5, 7, 29). We have, therefore, also investigated whether different specific clusters of transcription factors function within enhancers as discrete enhanceosome-like complexes.

We have employed the human granulocyte-macrophage colony-stimulating factor (GM-CSF) locus as a model to unravel the mechanisms utilized by diverse cell types to activate the same gene in a highly tissue-specific pattern (9). The GM-CSF gene can be activated by a variety of signaling pathways and is expressed inducibly in a diverse range of cell types that includes T cells, monocytes, mast cells, myeloid precursor cells, endothelial cells, fibroblasts, and epithelial cells. The GM-CSF gene is regulated by an inducible enhancer located 3 kb upstream of the GM-CSF gene that functions in most GM-CSF-expressing cell types (11). The enhancer is activated via protein kinase and calcium signaling pathways, which in T cells are coupled to the T-cell receptor.

The GM-CSF enhancer encompasses three composite NFAT/AP-1 elements, termed the GM330, GM420, and GM550 elements, which bind NFAT and AP-1 in a highly cooperative manner, in addition to the GM170 NFAT and AP-1 sites that do not function cooperatively (10) (as depicted in Fig. 2A below). The enhancer core also encompasses a Runx1 (AML1) site (GM450) and an Sp1-like element (GM300) (9). In recent studies, we demonstrated that, in T cells, enhancer function requires just the two centrally located NFAT/AP-1 elements (GM330 and GM420) that exist on adjacent nucleosomes (termed N1 and N2) (21) that span the conserved core region (9). Enhancer activation is accompanied by the rapid induction of a DNase I-hypersensitive (DH) site spanning these two specifically positioned nucleosomes, which

* Corresponding author. Mailing address: Experimental Haematology, Leeds Institute of Molecular Medicine, Wellcome Trust Brenner Building, St. James's University Hospital, Leeds LS9 7TF, United Kingdom. Phone: 44 113 3438639. Fax: 44 113 3438502. E-mail: p.n.cockerill@leeds.ac.uk.

† A.G.B. and B.V.J. contributed equally to this study.

‡ Present address: School of Molecular and Biomedical Sciences, University of Adelaide, Adelaide 5000, Australia.

▽ Published ahead of print on 5 February 2007.

become destabilized upon recruitment of NFAT/AP-1 complexes to the GM330 and GM420 elements. Enhancer function in T cells is absolutely dependent on the integrity of both the NFAT and AP-1 motifs within each of the GM330 and GM420 elements. An Sp1-like element (GM300) located just upstream of the GM330 element is also required for maximal activity.

Although the mechanism of NFAT function is unknown, there is evidence that it acts within the GM-CSF enhancer to promote nucleosome disruption and increase chromatin accessibility for other factors that bind the enhancer, including AP-1, Sp1, and Runx1, which all appear as in vivo footprints only in activated T cells (21). Furthermore, NFAT and AP-1 both have the capacity to specifically interact with CBP and P300, raising the possibility that NFAT/AP-1 complexes may function as multiprotein enhanceosomes (1, 7, 17).

The GM-CSF enhancer encompasses additional conserved sequences that extend immediately upstream of the essential core required for function in T cells (9) (see Fig. 2 below). One of these conserved regions includes two GATA-like elements, the GM170 AP-1 site, and an Ets-like element, which are all redundant for enhancer function in Jurkat T-cell transfection assays and lie outside of the DH site in T cells (21). However, we speculated that this region might direct an alternate mode of GATA-dependent transcription in erythroid/megakaryocytic lineage cells expressing GATA-1 and in mast cells expressing GATA-1 and GATA-2. In support of this model, we found that the GATA elements define the 3′ boundary of an upstream nucleosome (N0) that undergoes constitutive chromatin remodeling to form a DH site in myeloid cells that express GATA factors but not NFAT. In erythroleukemic and mast cell lines, the GATA elements were indeed required for enhancer function. In bone marrow-derived mast cells, we observed that GATA-2 binding to the enhancer was accompanied by repositioning of nucleosome N0 to a location 140 bp upstream from the position that it occupies in T cells and repositioning of the adjacent nucleosomes. Hence, this study reveals that the GM-CSF enhancer can function in a modular fashion, utilizing different sets of transcription factors in different cell types to establish alternate specific chromatin architectures and thus drive different expression patterns. These findings also imply that the transcription factors themselves dictate nucleosome positioning. We further demonstrate that enhancer activation was accompanied by a profound change in chromatin architecture over the flanking regions in both T cells and mast cells, where extensive nucleosome mobilization was observed.

MATERIALS AND METHODS

Transgenic mice. The GM-CSF transgenic mouse lines are as previously described (11) and contain a 10.5-kb XhoI-HindIII fragment spanning the gene, with or without the 717-bp BglII fragment of the enhancer. Transgene copy number was recalculated by both Southern blot analysis and real-time PCR to obtain the revised values presented in Fig. 1. Line C42 transgenic mice contain six copies of a 130-kb AgeI DNA fragment encompassing both the GM-CSF gene and the interleukin-3 (IL-3) gene, which is located 10 kb upstream of the GM-CSF gene. All studies of transgenic mice reported here have been performed with the consent of the local animal ethics committees and the U.K. Home Office.

Cell culture and preparation. Jurkat and CEM T cells, K562 and HEL erythroleukemic cells, HMC-1 mast cells, KG1a myeloblastic cells, HeLa cervical carcinoma cells, and human umbilical vein endothelial cells (HUVECs) were all cultured as previously described (3, 11, 18). HMC-1 mast cells were obtained from J. Butterfield (4). Human peripheral blood T cells and mouse splenic T cells were cultured for several days with IL-2, after an initial 2 days of culture with phytohemagglutinin or concanavalin A, respectively, to induce proliferation, as previously described (21). Transgenic mouse peritoneal cavity myeloid cells were obtained by peritoneal lavage with cold phosphate-buffered saline. Splenic monocyte/macrophage lineage cells were purified using CD11b (Mac-1) antibody magnetic beads (Miltenyi).

Human GM-CSF transgenic mouse mast cells were grown from adult femur and tibia bone marrow by culture in Iscove's modified Dulbecco's medium supplemented with 10% fetal calf serum (HyClone), 150 μM monothioglycerol, 500 U/ml penicillin and streptomycin, 10 ng/ml recombinant mouse IL-3 (Biosource), and 10 ng/ml recombinant mouse stem cell factor (SCF; R and D Systems). After 1 week, nonadherent cells were moved into a new flask and cultured at a density of 0.5×10^6 to 1×10^6 for a further 3 weeks with several changes of flask to remove any emerging adherent macrophages from the culture.

Mast cell analyses. Mast cells were stained using toluidine blue in 1% NaCl (pH 2.3) and were seen to have purple granules in the cytoplasm and round nuclei. Mast cell identity was further confirmed by fluorescence-activated cell sorting and cells stained positive using antibodies against c-Kit, CD34, and Sca-1, all of which are known to be expressed on mouse mast cells (14).

mRNA analyses. Human GM-CSF mRNA expression relative to mouse glyceraldehyde phosphate dehydrogenase (GAPDH) mRNA expression was measured by real-time PCR analysis with SYBR green as previously described (21). Primers used for the mouse GAPDH, Oct1A, Runx1, NFATc1, PU.1, GATA-1, and GATA-2 genes were designed using PCR Express and Oligo 5 software to anneal at 60°C. Standard curves for mRNA quantitation were prepared using serial dilutions of stimulated mast cell cDNA. The sequences used as primers were as follows: mOct-1A, GGACCAGCAGCTCACCTATCAA and CCG TACTGCTTGTCACAAGGCT; mRunx1, AGCGGTAGAGGCAAGAGCTTC and CGGATTTGTAAAGACGGTGATG; mNFATc1, TGGAAGCAAAGAC TGACCGG and CTGGTTGCGGAAAGGTGGTAT; mPU.1, CCATAGCGAT CACTACTGGGATTT and TGTGAAGTGGTTCTCAGGGAAGT; mGATA-1, GTCAGAACCGGCCTCTCATC and GTGGTCGTTTGACAGTTAGTGCAT; mGATA-2, TAAGCAGAGAAGCAAGGCTCGC and ACAGGCATTGCACAG GTAGTGG; and m c-*fms*, CTTTGGTCTGGGCAAGAAGAT and CAGGGCCT CCTTCTCATCAG.

ELISAs. Human and mouse GM-CSF protein concentrations were measured by enzyme-linked immunosorbent assay (ELISA) of the culture media, after stimulation of splenic cells or peritoneal cells, as previously described (11). Relative levels of GM-CSF transgene expression per gene copy were calculated as the ratio of human GM-CSF to mouse GM-CSF to transgene copy number, multiplied by 2 to correct for the mouse genome.

EMSAs. Electrophoretic mobility shift assays (EMSAs) were performed as described previously (21), using K562 nuclear extracts and the following probe and competitor sequences: GM138 GATA, CCCCTTGTGATAATGTCTCT CGT; GM153 GATA, TCTCTCGTGATAAGGATCCTGGA; GM-CSF promoter −114 GATA, GTGTGGCTGATAAGGGCCAGGAG; GATA consensus, CAGGGACATGATAAGGGAGCCAA; GM300 Sp1 site, TCGTGGTCC CCGCCTCTGCCCTGCC; GM-CSF promoter Sp1 site, AGTTCCCCCGCCT CCCTGGCATTTT; and Sp1 consensus, GCTCGCCCCGCCCCGATCGAATG.

Analysis of nuclease cleavage sites within nuclei. DNase I and micrococcal nuclease (MNase) digestions and analysis of chromatin fragments were performed essentially as previously described (21). DNase I (6 U/μg) and MNase were obtained from Worthington. The DH site analyses of human cell nuclei presented in Fig. 5A employed previously characterized DNase I-digested samples that represent optimally digested samples taken from series of DNase I titrations where we have previously demonstrated that we can efficiently detect constitutive and inducible DH sites (11). In each case, cells had been either not stimulated or stimulated for 4 to 6 h with 20 ng/ml phorbol myristate acetate (PMA) and 2 μM calcium ionophore A23187.

DNase I and MNase digestions of transgenic mouse T cells and mast cells were performed using isolated nuclei as described previously (21), with the exception that digestions of activated mast cells were performed on permeabilized cells rather than nuclei. This approach was necessary here because nuclei from activated mast cells were too fragile to permit purification of nuclei. To confirm that permeabilization does not itself alter the results, we demonstrated that the same cleavage patterns could be obtained with permeabilized T cells as in purified T-cell nuclei. Permeabilized cell digestions were performed by first suspending mast cells to a concentration of 3×10^7 to 4×10^7 cells/ml in nuclei digestion buffer (60 mM KCl, 15 mM NaCl, 5 mM $MgCl_2$, 10 mM Tris [pH 7.4], 0.3 M sucrose) at 22°C. Digestions were then performed by adding the enzyme in an equal volume of digestion buffer containing 2 mM $CaCl_2$ and 0.4% Nonidet P-40

and digesting for 3 min at 22°C. High-resolution mapping of nuclease cleavage sites in the GM-CSF enhancer was performed by indirect end labeling using either a PshAI-HindIII fragment upstream of the enhancer or a SalI-PshAI fragment within the GM-CSF gene for PshAI-digested samples run on 1.2% agarose gels or a BglII-BglI fragment downstream of the enhancer for BglI-digested samples run on 1.5% agarose gels. Low-resolution mapping of DH sites 5′ of the GM-CSF gene (using EcoRI) and 3′ of the IL-3 gene (using BamHI) was performed as previously described (11). For the above indirect end-labeling assays of mast cells and T cells, nuclease digestions were performed using 15 to 40 U/ml MNase and 5 to 15 μg/ml (~30 to 100 U/ml) DNase I for 3 min.

Analyses of mono- and oligonucleosome fragments by Southern blot hybridization were performed using 2% agarose gels and alkaline transfer (in 0.5 M NaOH plus 1.5 M NaCl) to GeneScreen Plus (Perkin-Elmer) nylon membranes as described previously (21), using 1.5 μg of DNA samples obtained from chromatin digested within the range of 50 to 500 U/ml MNase for 3 to 15 min at 22°C. Specific nucleosomal regions were probed using the N2 probe described previously (21), and PCR generated fragments using the N0 primers TCTCAGGTC CCCAGAGATAACAAG and GGGCTGATCTGATCCTTCTTTG and the primers located 1.3 kb upstream of the gene (−1.3-kb primers) GACCACAGT GCTAAAGCCATGA and GGTTGGACACAAGCGAGAACA. The 3′ end of the locus (+4.0 to +4.8 kb) was probed using a 0.85-kb BglII-HindIII fragment.

All imaging and densitometry of hybridization patterns were performed using a Bio-Rad FX phosphorimager and Quantity One software to collect images and traces of digestion patterns. Excel software (Microsoft) was used to digitally calculate ratios between each point on the traces derived from chromatin digestions and DNA control digestions and to transform migration distances within lanes to sizes in base pairs via an equation derived from mobilities of the restriction enzyme fragments.

ChIP. Chromatin immunoprecipitation (ChIP) assays were performed essentially as published in reference 2, with the following minor modifications. Cells were fixed in 0.33 M (1%) formaldehyde for 5 min, before adding 5 volumes of phosphate-buffered saline containing 0.125 M glycine, to provide a twofold molar excess of glycine over formaldehyde. DNA was purified after proteinase K digestion using QIAGEN PCR purification columns. ChIPs employed 5 μg of antibodies recognizing either mouse and human GATA-2 (sc-9008; Santa Cruz Biotech), acetyl histone H3 K9 (07-352; Upstate Biotechnology), pan-acetyl istone H4 (06-598; Upstate Biotechnology), or unmodified histone H3 (1791-100; Abcam). Control ChIPs employed purified normal rabbit immunoglobulin G (IgG) (12-370; Upstate Biotechnology). Real-time PCR was used to determine the amount of each gene-specific amplicon present. All values were determined from standard curves using input DNA (DNA purified from sonicated chromatin before ChIP). All ChIP data were normalized by expressing the amount of each specific DNA precipitated as a ratio with the values obtained using a region of mouse chromosome 1. This control was selected on the basis that it is located within an extensive gene-free region, is free of repetitive or conserved sequences, and is at least 200 kb from the nearest known transcribed sequence. As a positive control, we selected the intronic enhancer from the IL-4 gene which is known to bind GATA-2 in mast cells in vivo (24). For negative controls, we employed (i) a region 1.5 kb upstream of the c-*fms* promoter, which we confirmed was inactive in mast cells, and (ii) a region 17 kb upstream of the mouse PU.1 gene.

The sequences of the primers were as follows: m IL-4 intron 2, AACCACC CCACAGGTCTTTGTT and TGAAAGGCCCCAAAGTCTTGA; m c-*fms* −1.5 kb, CACGCCGGCTGAGTGTCT and TCCACGTAGATGGTGTCAG CAT; m chromosome 1 control sequence, TGCTCCACAGTGTCCATGTACA and AGCAATTTCATGGGTGAGAGAAG; h GM-CSF enhancer, GGAGCC CCTGAGTCAGCAT and CATGACACAGGCAGGCATTC; h GM-CSF promoter, TGTCGGTTCTTGGAAAGGTTCA and TGTGGAATCTCCTGGCC CTTA; and m PU.1 −17 kb, CCTCCCAAGTGCTGGGATTAA and TGAGC ACACGAACACACTTAAGTGTA.

Transient transfection assays. Transfection assays and luciferase assays were performed using the luciferase reporter gene plasmid pXPG plus either just the bp −627 to +28 segment of the human GM-CSF promoter (pXPG-GM627) or the promoter plus the 717-bp fragment of the human GM-CSF enhancer (pXPG-GM627-B717), with and without point mutations, as described previously (21). The plasmid derivatives BM575, BH355, BA260, AM315, and HM231 contain the enhancer fragments depicted in Fig. 4 in place of the BglII fragment.

RESULTS

The long-term goal of these studies is to gain an understanding of how alternate tissue-specific mechanisms combine to establish GM-CSF gene expression in multiple cell lineages. We also aim to determine and compare the consequences of recruitment of different classes of transcription factors to the same enhancer, in terms of nucleosome positioning and remodeling. These studies first require the development of appropriate model systems, which will then be used for detailed structural and functional studies.

The GM-CSF enhancer is essential for GM-CSF gene expression in myeloid cells. We previously determined that the GM-CSF enhancer is required for efficient GM-CSF gene expression in spleen cells derived from human GM-CSF transgenic mice (11). While T cells represent the main source of GM-CSF expression in the spleen, in this study we aimed to identify an additional role for the GM-CSF enhancer in the myeloid compartment and to determine whether it functioned by the same mechanisms in these different cell types.

We first investigated GM-CSF enhancer function in both spleen cells and a mixed population of myeloid cells recovered from the peritoneal cavity of GM-CSF transgenic mice. The peritoneal population primarily includes GM-CSF-expressing cell types such as monocytes and macrophages. Cells were obtained from both the peritonea and spleens of seven lines of transgenic mice containing the intact 10.5-kb GM-CSF locus and six lines of GM-CSF transgenic mice lacking the enhancer (ΔE GM-CSF) (Fig. 1A). Human and mouse GM-CSF expression levels were assayed by ELISA after stimulation with phorbol ester and calcium and calcium ionophore (PMA/I) (Fig. 1B). These agents act predominantly to activate kinase pathways that induce AP-1 and NF-κB and calcium pathways that induce NFAT, although there is also a lot of cross talk between these pathways in the activation of these factors.

In the spleen, the activity per gene copy of the intact human GM-CSF locus was equal to or greater than that of each copy of the endogenous mouse GM-CSF gene (Fig. 1B). Transgenes lacking the enhancer were on average 14% as active as the intact transgenes. In the peritoneal cells, the intact human GM-CSF gene was several times more active than the mouse GM-CSF gene. In these myeloid cells, deletion of the enhancer almost abolished gene activity, reducing average expression levels to just 2.6% of that of the wild-type transgene. Similar results were obtained with peritoneal cells enriched for macrophages by adherence to culture dishes (data not shown).

In myeloid cells, cytokine gene activation can also be triggered by bacterial lipopolysaccharide (LPS) via Ca^{2+}-independent pathways that induce AP-1 and NF-κB. To determine whether the GM-CSF enhancer could also be activated via these pathways, we assayed transgene expression in peritoneal cells stimulated with LPS. The intact transgene was induced by LPS to a level similar to that of the endogenous GM-CSF gene, and loss of the enhancer reduced expression levels to just 1% of wild type on average (Fig. 1). Hence, the enhancer appears to be essential for GM-CSF expression induced in myeloid cells by both NFAT-dependent and -independent pathways.

We next purified CD11b-positive myeloid cells from the spleens of several of our lines of GM-CSF transgenic mice. These cells represent primarily monocyte/macrophage lineage cells and account for about 5% of the cells in the spleen. Cells were stimulated for 4 h with PMA/I, and the levels of GM-CSF transgene mRNA expression were determined relative to mouse *Gapdh* mRNA expression. Mirroring the above observations, the intact GM-CSF locus was induced to similar levels

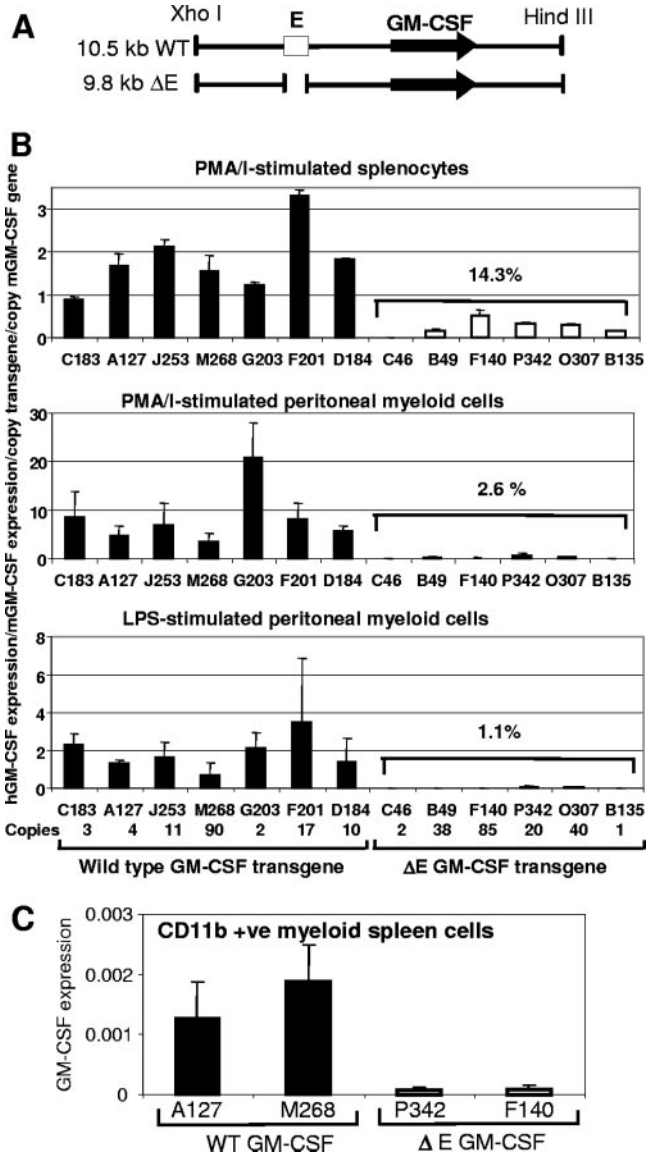

FIG. 1. GM-CSF expression in GM-CSF transgenic mice. (A) GM-CSF transgenes with and without the enhancer. WT, wild type. (B) ELISAs of human GM-CSF expression expressed relative to mouse GM-CSF expression, divided by transgene copy number and multiplied by 2 to correct for mouse GM-CSF copy number. GM-CSF was measured in culture supernatants from splenocytes and peritoneal myeloid cells stimulated for 15 h with 20 ng/ml PMA and 1 μM A23187 (PMA/I) or 10 μg/ml LPS. Transgene copy numbers are displayed below. Black bars depict wild-type transgenes, and open bars depict transgenes lacking the enhancer. Error bars represent standard error (SE). (C) Human GM-CSF mRNA expression in CD11b-positive GM-CSF transgenic splenocytes stimulated for 4 h with 20 ng/ml PMA and 2 μM A23187. mRNA expression was measured by real-time PCR of cDNA and is expressed relative to mouse GAPDH expression and corrected for transgene copy number. Error bars represent SE. +ve, positive.

of expression in two independent lines of mice, whereas transgene expression was almost eliminated in mouse lines lacking the GM-CSF enhancer (Fig. 1C). However, the level of GM-CSF mRNA expression in splenic myeloid cells was only about 0.1 to 0.2% of that of *Gapdh*. This is in marked contrast to activated T cells, which express approximately the same levels of GM-CSF and *Gapdh* mRNA (data not shown).

The GM-CSF enhancer and promoter encompass GATA and Sp1 elements. Most myeloid cell types (other than macrophages) employ GATA family transcription factors to drive differentiation and specific gene expression. These include myeloid precursor cells, mast cells, erythroid cells, megakaryocytes, and eosinophils, which express GATA-1 and/or GATA-2 to various degrees, with GATA-1 most prominent in erythroid cells and GATA-2 most prominent in mast cells (31). It is, therefore, highly significant that the GM-CSF enhancer also encompasses two stretches of conserved sequence which lie just upstream of the core elements that function in T cells and include two conserved ideal consensus GATA elements (Fig. 2). These two closely coupled GATA sequences (TGATAAT and TGATAAG) reside between a conserved Ets-1-like consensus sequence and the downstream GM170 AP-1 site (Fig. 2B). We defined these GATA-like sequences as the GM138 and GM153 elements, according to their location within the 717-bp BglII enhancer fragment, in line with the convention used for all elements within the GM-CSF enhancer. To determine whether these two elements function as genuine GATA sites, we performed EMSAs with nuclear extracts prepared from the erythroleukemic cell line K562, which expresses high levels of GATA-1. The GM138 and GM153 probes each functioned as highly efficient GATA-1-binding elements that could both compete for GATA-1 binding and be blocked by a GATA consensus sequence (Fig. 2D).

We also performed EMSAs on a conserved GATA-like element (TGATAAG) that is located in the GM-CSF promoter 114 bp upstream of the transcription start site. This sequence also functioned as an efficient GATA-1-binding element (Fig. 2D). We performed additional GATA EMSAs to define cell lines representing useful models that express high or low levels of GATA family factors (Fig. 2E). The HMC-1 mast cell line expressed significant levels of GATA-like factors, which comigrated with the K562 GATA-like complexes, whereas Jurkat and CEM T cells both expressed much lower levels. Because GATA elements frequently cooperate with Sp1 sites, we performed additional EMSAs with Sp1-like elements located in the GM-CSF enhancer (GM300) and promoter (9). These assays confirmed that both sites functioned as efficient Sp1 sites when assayed in parallel with an ideal consensus Sp1 site (Fig. 2F).

Mast cells as a model for GATA-dependent GM-CSF gene regulation. Mast cells are known to utilize both GATA and NFAT family transcription factors in the regulation of other cytokine genes located near the GM-CSF locus (24, 30), and GATA-2 is a major factor directing mast cell differentiation (35). To prepare an enriched population of mast cells, we cultured nonadherent bone marrow cells in the presence of IL-3 and SCF for approximately 4 weeks. The resulting cells resembled mature differentiated mast cells in that they were uniformly packed with toluidine blue staining granules and were essentially 100% Sca-1, CD34, and c-Kit positive (data not shown) (14). We confirmed that these cells represented an appropriate model for studying mechanisms of GM-CSF enhancer regulation by demonstrating (i) that they expressed high levels of the transcription factors GATA-1, GATA-2, Runx1, and NFATc1 relative to the ubiquitous factor Oct-1

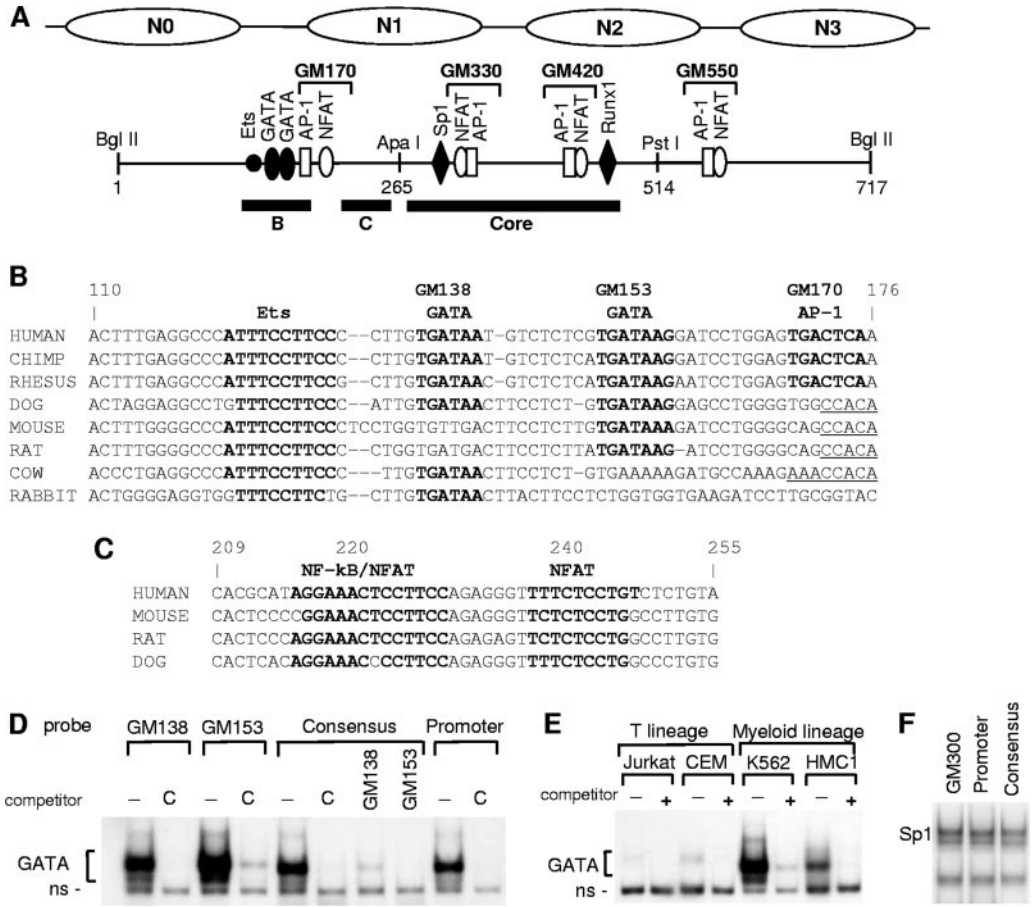

FIG. 2. GATA-2 binding at the human GM-CSF enhancer. (A) Map of the GM-CSF enhancer showing previously defined transcription factor binding sites plus predicted Ets and GATA sites. The sequence is numbered relative to the BglII site defining the 5′ boundary of the enhancer. Brackets indicate the defined composite NFAT/AP-1 binding sites located at 170, 330, 420, and 550 bp relative to the 5′ BglII site. The positions of specific defined nucleosomes as measured in T cells are shown above. Depicted underneath are the blocks of conserved sequences displayed in panels B and C and the conserved core region that is required for enhancer function in T cells. (B) Alignment of the human GM-CSF enhancer sequence from positions 110 to 176 bp (relative to the 5′ BglII site) with homologous sequences in the chimpanzee, rhesus monkey, dog, mouse, rat, cow, and rabbit genomes. The Ets-1-like sequence and at least one of the two GATA elements are conserved in all species presented. Each of the GATA elements and the GM170 AP-1 site are all conserved in primates, but not in other species. Highly conserved predicted regulatory elements are shown in boldface. The underlined sequences depict a Runx1-like element that exists in place of the AP-1 site in some species. (C) Alignment of the sequence from bp 209 to 255 of the human GM-CSF enhancer with the mouse, rat, and dog genomic sequences shows conservation of the NF-κB and NFAT-like elements in this region. (D) EMSAs of GATA elements within the GM-CSF enhancer and promoter, performed with 5 μg of K562 nuclear extract and 0.2 ng of probe, in the presence and absence of 20 ng of oligonucleotide duplex competitor, in the form of either the GATA consensus sequence (labeled C) or the GM138 or GM153 GATA sequences. (E) EMSAs performed as in panel D using nuclear extracts from the indicated cell lines, in the presence and absence of the GATA consensus competitor. (F) EMSAs of Sp1 sites in the GM-CSF enhancer and promoter, assayed in parallel with a consensus Sp1 sequence. ns, nonspecific complex.

(Fig. 3A) and (ii) that they expressed very high levels of GM-CSF mRNA expression relative to *Gapdh* mRNA after stimulation with PMA/I (Fig. 3B). The relative level of GM-CSF gene expression in mast cells was approximately 10^4-fold higher than that detected in splenic CD11b-positive myeloid cells (Fig. 1C) and severalfold higher than that detected in transgenic T cells (data not shown). This suggests that mast cells and T cells represent more meaningful sources of GM-CSF than monocyte-macrophage lineage cells. Significantly, we showed that the GM-CSF enhancer was essential for GM-CSF gene expression in mast cells because transgenes lacking the enhancer expressed almost undetectable levels of GM-CSF mRNA (Fig. 3B). We also demonstrated that the enhancer existed as a highly inducible DH site in mast cells, but in contrast to T cells (21), it also existed as a weak DH site prior to stimulation (Fig. 3C), suggesting a different pattern of regulation. For DNase I control purposes, we performed a parallel analysis of a cluster of DH sites located just downstream of the IL-3 gene (Fig. 3C) that includes three ubiquitous constitutive DH sites and one inducible site (9). This analysis confirmed that the two samples were digested to similar extents by DNase I and demonstrated that the IL-3 kb +4.5 DH site is also inducible in mast cells. Note that the GM-CSF promoter appears to be decrease in hypersensitivity after stimulation (Fig. 3C) as a result of the increased cleavage at the enhancer which eliminates the longer fragments. In contrast, the analyses described below in Fig. 6 demonstrate that hypersensitivity at the promoter actually increases after stimulation.

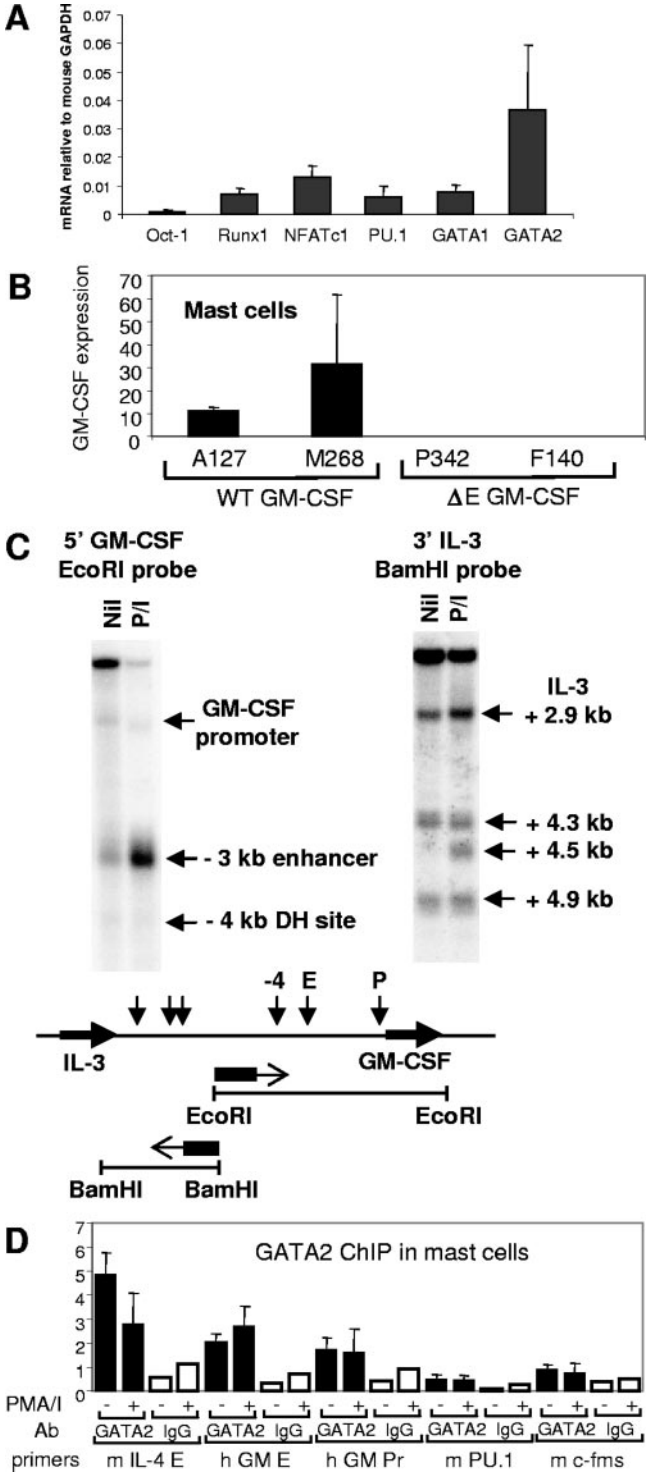

FIG. 3. Characterization of mouse mast cells. (A) Real-time PCR analysis of mouse transcription factor mRNA expression in mast cells. PCRs were performed on mast cell cDNA, and mRNA levels were expressed relative to mouse GAPDH as in Fig. 1. Note that all of the tissue-specific transcription factors measured here are expressed in levels greater than that of the ubiquitous transcription factor Oct1A. (B) Human GM-CSF mRNA expression in GM-CSF transgenic mast cells stimulated for 4 h with 20 ng/ml PMA and 2 μM A23187. mRNA expression was measured by real-time PCR of cDNA and is expressed relative to mouse GAPDH expression and corrected for transgene copy number. Error bars represent standard deviation. WT, wild type. (C) Analysis of DH sites within the enhancer (E) and promoter (P) upstream of the GM-CSF gene. DNase I digestions were performed on permeabilized mast cells grown from bone marrow obtained from line C42 transgenic mice carrying the intact IL-3/GM-CSF locus. Cells were either unstimulated (nil) or stimulated for 4 h with 20 ng/ml PMA and 2 μM A23187 (P/I). Mapping of DH sites was performed from the indicated EcoRI or BamHI sites using the probes depicted by boxes, as previously described (11). The BamHI probe was used to detect a cluster of ubiquitous constitutive and inducible DH sites (11) so as to control for the extent of DNase I digestion, and the samples analyzed here represent just the optimum digestion points selected from a DNase I titration series. (D) ChIP assays of GATA-2 binding in M268 transgenic mast cells at the GM-CSF enhancer (GME) and promoter (GM Pr). Columns represent the amount of genomic DNA precipitated using a polyclonal GATA-2 antibody (black bars) or a normal rabbit IgG (open bars) from chromatin prepared from unstimulated cells (−) and cells stimulated for 4 h with 20 ng/ml PMA and 2 μM A23187 (+). Values are expressed relative to an inactive control region located on mouse chromosome 1. mIL-4 E depicts the mouse IL-4 intron 2 enhancer, which binds GATA-2, whereas mouse (m) *PU.1* and c-*fms* are negative control amplicons, as detailed in Materials and Methods. Error bars indicate standard deviation.

To determine whether the GM-CSF enhancer and promoter GATA elements functioned as GATA-binding sites in vivo, we performed ChIP assays on mast cells with GATA-2 antibodies. As a positive control, we used the GATA-2-regulated intronic enhancer of the IL-4 locus (24) and we used inactive regions of the mouse *PU.1* and c-*fms* loci as negative controls (Fig. 3D). For a normalization control, we employed a nonconserved sequence centered within a 400-kb transcript-free region located on mouse chromosome 1. The GATA-2 ChIP analyses revealed significant GATA-2 binding to the GM-CSF enhancer and promoter and the IL-4 intronic enhancer and background levels in the inactive controls in both stimulated and unstimulated mast cells. This constitutive in vivo binding of GATA-2 in nonstimulated mast cells may account for the presence of weak constitutive DH sites seen in the enhancer and promoter in nonstimulated cells (Fig. 3C).

The GM-CSF enhancer is modular and is differentially regulated in T cells and myeloid cells. The transcription factor binding sites in the GM-CSF enhancer are organized as discrete clusters of sites that potentially function as differentially regulated enhanceosome-like complexes. To assess the degree of tissue specificity and the cooperativity of the different regions of the enhancer, we performed transient transfection assays using GM-CSF promoter/enhancer luciferase reporter gene plasmids (Fig. 4) in a panel of myeloid and T-cell lines that express GATA and/or NFAT family proteins. This panel included Jurkat and CEM T cells that each express NFAT but little GATA protein, K562 and HEL pro-erythroid/megakaryocytic cells that express GATA-1 but little NFAT, and HMC-1 mast cells and KG1a CD34-positive primitive myeloid cells that express both families of factors (Fig. 2E) (3; data not shown).

The first set of luciferase reporter gene constructs tested each contained the bp −627 to +28 fragment of the human GM-CSF gene promoter (GM627), with or without different combinations of the three major clusters of regulatory elements that exist within the enhancer (Fig. 4A). The 575-bp BglII/MscI segment (BM575) encompasses all of the known

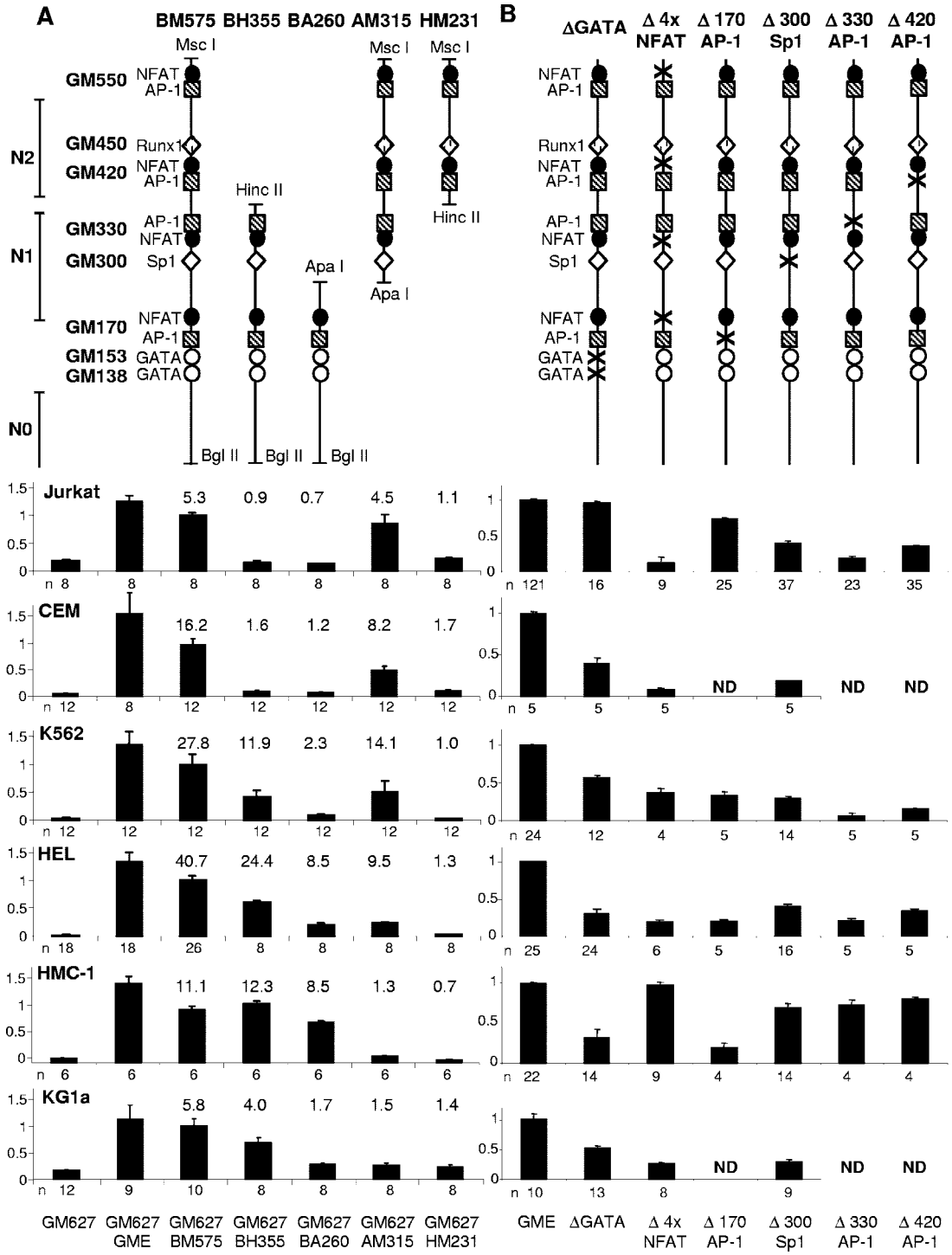

FIG. 4. The GM-CSF enhancer is composed of distinct tissue-specific modules. GM-CSF enhancer deletions and mutations were assayed in transient transfection assays. Cells were transfected with 5 μg of DNA, cultured for a further 20 h, and then stimulated for 9 h with 20 ng/ml PMA and 2 μM A23187. Constructs were based on the human GM-CSF promoter/luciferase gene plasmid pXPG-GM627 and contain the 717-bp BglII segment of the GM-CSF enhancer (GME) (pXPG-GM627-B717) with or without point mutations, or the indicated subsegments of the enhancer, inserted upstream of the promoter (21). Enhancer subfragments (A) and enhancer mutations (B) were assayed separately. Values in panel A are expressed relative to BM575, with the increase (fold) over the promoter alone displayed above each column, and values in panel B are expressed relative to GME. Each column represents the average of transfections of at least two independent clones of each construct. The numbers of individual transfections are displayed under each column, and error bars represent standard error. ND, not determined.

binding sites and nuclease-sensitive regions and functioned as an inducible enhancer to essentially the same extent as the previously defined 717-bp BglII fragment (GME) in all of the cell lines tested. These constructs only supported near-background levels of activity in the absence of stimulation (data not shown). In these studies, it was also significant that the relative activity of the enhancer compared to that of the promoter alone was five- to eightfold greater in the GATA-1-expressing cell lines K562 and HEL than it was in Jurkat cells.

A truncated 315-bp ApaI/Msc I segment (AM315) that encompasses the GM330 and GM420 elements retained full enhancer activity in Jurkat T cells. However, this segment lacks the GATA/GM170 region and had little activity in the HEL, HMC-1, and KG1a myeloid cell lines and reduced activity in CEM and K562 cells. Conversely, the BglII/HincII segment (BH355), which includes the GATA, GM170, and GM330 elements but not the GM420 element, had no activity in the Jurkat and CEM T-cell lines but retained full or substantial activity in all of the myeloid cell lines. The BA260 and HM231 constructs lacking the central GM330 region were essentially inactive in most cases, except for HMC-1 cells, where the BA260 GATA region was sufficient for significant enhancer function.

To identify roles for individual elements in the enhancer, we performed site-directed mutagenesis in the context of the 717-bp BglII fragment inserted in pGM627 (Fig. 4B). In line with the above results, mutation of the GATA elements had no effect in Jurkat cells but decreased enhancer activity in all of the other cell lines tested. The combined mutation of all four defined NFAT sites abolished activity in Jurkat and CEM T cells, but had no effect in HMC-1 cells and intermediate effects in the other cell lines. Mutation of just the GM420 NFAT site also abolished activity in Jurkat and CEM T cells, but had little or no impact in KG1a or HMC-1 cells (data not shown). Mutations in individual AP-1 sites had very specific effects depending upon their context. The GM170 AP-1 site adjacent to the GATA elements was required for function in GATA-expressing K562, HEL, and HMC-1 cells, but not in Jurkat cells. Conversely, the GM330 and GM420 AP-1 sites, which are both linked to NFAT sites, were essential for function in Jurkat T cells but played no role in HMC-1 cells. This indicates that the different AP-1 sites must cooperate in a specific differentially regulated manner with neighboring sites. The Sp1 site contributed to function in every cell type, but was not essential. There was, however, no effect from mutations in the GM170 or GM550 NFAT sites, the GM450 Runx1 site, or the Ets-like element in any of the cell lines (data not shown).

The GATA region of the GM-CSF enhancer forms a distinct DH site in myeloid cells. Active regions within enhancers and promoters are commonly associated with discrete domains of chromatin remodeling that are detected as DH sites. In order to obtain evidence whether specific enhancer modules in the endogenous GM-CSF gene are active in different cell types, we proceeded to map DH sites in the cells used in the above studies. In addition, we included peripheral blood T cells, which express GM-CSF and NFAT; HUVECs, which express GM-CSF, NFAT and GATA factors; and HeLa carcinoma cells, which express GM-CSF but not GATA or NFAT. DH sites were mapped at high resolution across the GM-CSF enhancer from a PshA1 site located 1.5 kb upstream of the BglII site that defines the 5′ boundary of the enhancer (Fig. 5A and B). In all T lineage cells, the DH site was only present in stimulated cells, and was confined to nucleosomes N1 and N2, which encompass the GM330 and GM420 elements. This region is roughly defined by the ApaI and PstI sites and includes all of the sites known to be required for enhancer function in T cells (21). In myeloid cells, the DNase I mapping revealed distinctly different patterns of DH sites. Significantly, the GATA-1- and/or GATA-2-expressing K562, HEL, and HMC-1 cells each had a novel myeloid-specific DH site spanning the GATA elements and nucleosome N0 that reside between the ApaI and 5′ BglII sites, and this site was detected in both stimulated and unstimulated cells. (In parallel experiments, this site was maintained in the same position in activated HEL cells [data not shown].) This lower myeloid-specific DH site was in some cases accompanied by an upper DH site equivalent to the inducible site seen in T cells.

Stimulated endothelial cells (HUVECs), which express both GATA and NFAT family proteins, also had two DH sites spanning the GATA and GM330/GM420 regions. KG1a cells, however, presented a uniquely different pattern. KG1a cells had no constitutive DH site, but had a broad inducible DH site spanning the ApaI site and including the novel NF-κB and NFAT-like elements at positions 220 and 240 (that were identified as conserved elements in Fig. 2C), but not extending into the nucleosome N0 region. Activated HeLa cells had a single sharply defined DH site centered between nucleosomes N1 and N2, midway between the ApaI and PstI sites.

The pattern of chromatin remodeling largely reflected the pattern of DNA element utilization in each cell type and provided further evidence for distinct mechanisms of gene regulation being employed in different lineages. The myeloid-specific DH site spans several conserved known and potential transcription factor binding sites (Fig. 2). Although this study has concentrated on the role of the GATA elements, it is noteworthy that this region also encompasses the GM170 NFAT and AP-1 elements, the highly conserved Ets-like sequence (of unknown function) just upstream of the GATA sites, and the highly conserved NF-κB and NFAT-like elements at positions 220 and 240.

Differential regulation of nucleosome positioning and chromatin remodeling across the GM-CSF enhancer in mast cells and T cells. To investigate the impact of distinct tissue-specific mechanisms of transcription factor recruitment on chromatin remodeling in normal cells, we performed very-high-resolution DNase I and MNase mapping of the chromatin structure of the GM-CSF enhancer in GM-CSF transgenic T cells and mast cells. These analyses revealed that the in vivo association of GATA-2 with the enhancer in mast cells has profound consequences for nucleosomal organization within the enhancer and identified different inducible patterns of nucleosome reorganization in mast cells and T cells. DH sites and MNase cleavage sites were mapped in stimulated and unstimulated cells from the BglI site located 660 bp downstream of the enhancer (Fig. 5B and C), and band sizes were calculated from the mobilities of the restriction enzyme fragments. The positions of prominent MNase bands, numbered relative to the 5′ BglII site of the enhancer (which is located at −3289 relative to the transcription start site), are shown to the right (Fig. 5C).

MNase and DNase I digestion of mast cell nuclei revealed

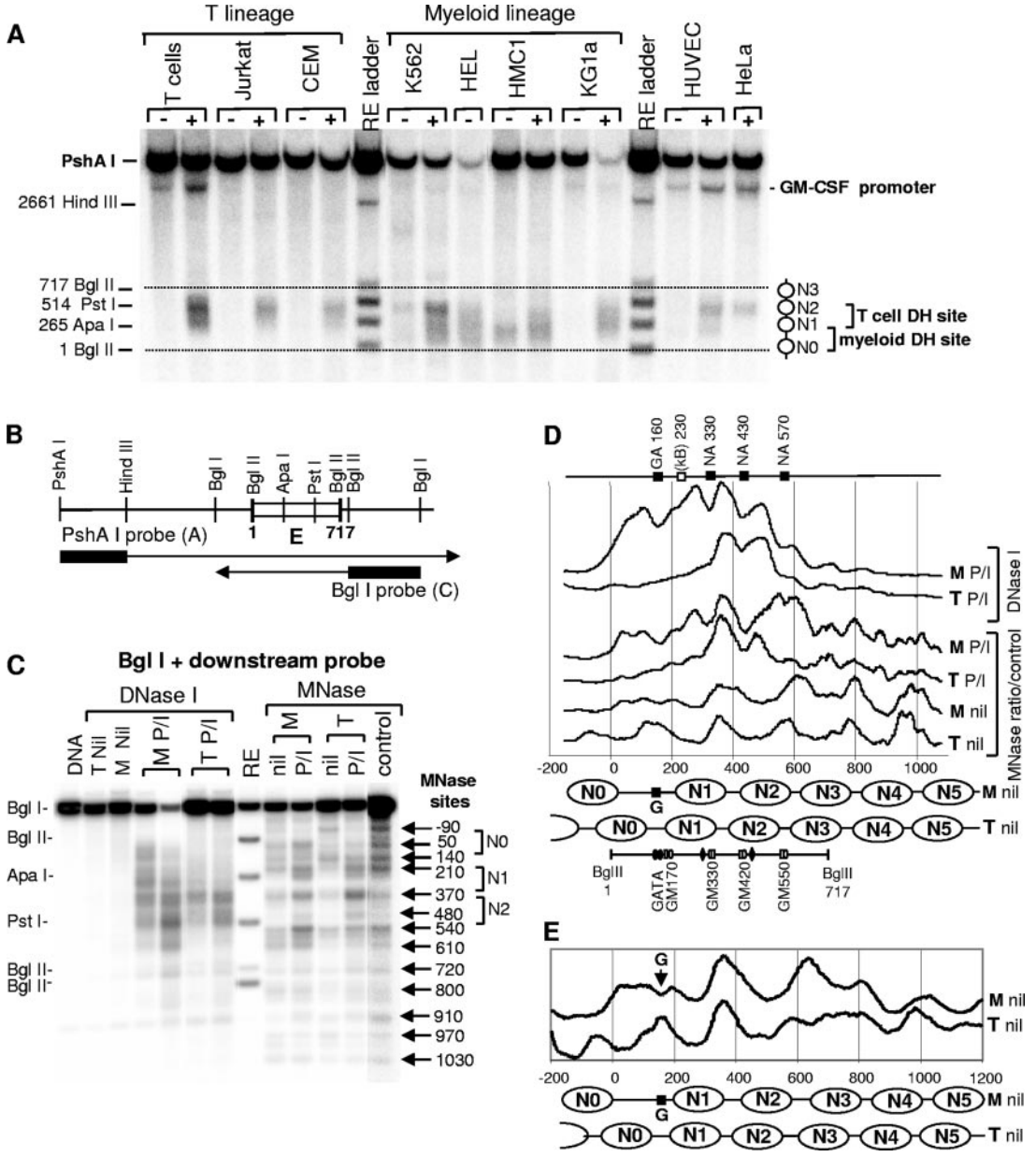

FIG. 5. Mast cells and T cells adopt a different chromatin architecture at the GM-CSF enhancer. Analysis of nuclease sensitivity within the GM-CSF enhancer by Southern blot hybridization. (A) DH sites were assayed by indirect end labeling from the 3′ PshA I site, using the probe depicted in panel B, in the indicated cells and cell lines before (−) and after (+) stimulation with 20 ng/ml PMA and 2 μM A23187 for 4 to 6 h. The restriction enzyme (RE) ladder is a mixture of PshAI-digested genomic DNA samples, also digested with either PstI, ApaI, or HindIII or partially digested with BglII. (B) Map of the GM-CSF enhancer region (open box) depicting the PshAI-HindIII and BglII-BglI probes used for mapping in panels A and C. (C) DH sites and MNase sites were assayed in cultured splenic T cells (T) and bone marrow-derived mast cells (M) from the human GM-CSF transgenic line M268, before (nil) and after (P/I) stimulation with 20 ng/ml PMA and 2 μM A23187 for 4 h. For DNase I digestions of stimulated cells, the right-hand lane of each pair represents a higher concentration of DNase I. Cleavage sites were mapped from the 3′ BglI site using the probes depicted in panel B. Numbers to the right indicated the positions of major MNase bands relative to the 5′ BglII site. The first lane (DNA) represents genomic DNA. The last lane (control) represents genomic DNA digested with MNase. (D) Graphs of either actual DNase I cleavage (top two traces) or relative MNase cleavage (bottom four traces) detected in BglI-digested samples in panel C plotted according to the positions of cleavage sites relative to the 5′ BglII site. Relative MNase cleavage was calculated by dividing the intensity of signal at each point by the signal obtained for the control MNase digest at the same point. Regions where there is evidence for protection from nuclease cleavage are shown as boxes above the panel, together with the positions of these protected regions and a prediction of factors that may be bound at these sites (N, NFAT; A, AP-1; G, GATA-2; and κB, NF-κB). Nucleosome positions predicted from the graphs are indicated below. (E) Graphs derived from Fig. 6A of relative MNase cleavage within the enhancer detected in PshAI-digested samples probed from the upstream probe (B).

complex specific cleavage patterns with nuclease-hypersensitive sites spanning nucleosome N0 and the N0/N1 linker region which were essentially absent in T cells. Additional strong nuclease-hypersensitive sites associated with the nucleosomes N1 and N2 were present in both the activated T cells and the activated mast cells. Hence, chromatin remodeling in T cells appears to be restricted to just the GM330 and GM420 regions, whereas all known regulated elements within the enhancer become remodeled in activated mast cells and form a 600-bp hypersensitive region.

As the first stage of a detailed analysis of the chromatin structure data presented here, we remapped the positions of nucleosomes in both mast cells and T cells. Because MNase exhibits pronounced sequence specificity, we further refined these analyses by employing densitometry and digitally calculated the relative sensitivity of MNase cleavage within each lane in Fig. 5C. We calculated the ratios of MNase digestion of chromatin samples compared to a genomic DNA digest and then replotted both the relative MNase sensitivity and the absolute DNase I sensitivity as a function of size. The ratios determined from the BglI analyses of MNase digests of stimulated and unstimulated mast cells and T cells (Fig. 5C) are presented as the lower four graphs in Fig. 5D. In unstimulated T cells, the analyses of relative MNase cleavage revealed a strikingly regular specific positioning and ~200-bp periodicity of nucleosomes across the enhancer and extending into the flanking sequences (Fig. 5D). The predicted nucleosome positions are displayed underneath the traces in Fig. 5D and differ only marginally from our previous less-refined analysis of nucleosome positions (21). From these maps (and from the additional analyses presented below in Fig. 6), we can define approximate positions (shown in parentheses) in T cells for nucleosomes N-1 (−230 to −70), N0 (−40 to 120), N1 (180 to 340), N2 (380 to 540), N3 (600 to 760), and N4 (800 to 960). These data confirm that the GM330 and GM420 NFAT/AP-1 elements lie within nucleosomes N1 and N2, respectively, and that the GATA elements must lie within a broad linker region separating nucleosomes N0 and N1.

In mast cells, the nucleosome N0 region and its 3′ linker adopted a structure distinctly different from that seen in T cells. Nucleosome N0 was essentially excluded from its previously determined location and was either evicted or shifted to a new position approximately 140 bp upstream (approximately −180 to −20) and replaced by an extensive MNase-hypersensitive (MH) region spanning the GATA elements, with a short protected region at position 160 where the GATA sites reside (Fig. 5C and D). Downstream of the GATA region, nucleosomes also existed in slightly different positions from those seen in T cells, being located ~30 bp further downstream (N1, 210 to 370; N2, 410 to 570; N3, 630 to 790; and N4, 820 to 980). These findings were confirmed by subsequent analyses (to be presented in full below in Fig. 6) mapping enhancer nucleosome positions from an upstream PshAI site, which are summarized in Fig. 5E. These studies demonstrate that the same nucleosome positions are predicted regardless of whether positions were mapped from upstream or downstream (Fig. 5D and E). Significantly, these observations reveal that transcription factors can play a major role in defining nucleosome positions within an array of nucleosomes, even before an enhancer has become activated.

In both mast cells and T cells, enhancer activation was associated with the appearance of MH sites across the GM330 and GM420 regions and extensive disruption of the organization of the regular nucleosome array in the sequences flanking the enhancer (Fig. 5D). In addition, prominent inducible MH sites flanking the GATA region were seen in activated mast cells but not in T cells. Densitometric traces of DNase I cleavage within the DH sites in activated mast cells and T cells are also displayed above the MNase traces in Fig. 5D. It is striking that the pattern of DH sites closely mirrors the pattern of MH sites, and the overall pattern suggests that nucleosomes are either absent or extensively disrupted in all of the regions where factors are predicted to bind. Hence, for both MNase and DNase I digests, distinct protected regions are seen that correspond to the GM330, GM420, and GM550 NFAT/AP-1 elements in activated mast cells and T cells and at the conserved GATA region specifically in activated mast cells. Also just visible in the traces of the activated mast cell MNase and DNase I analyses is a weakly protected region at position 230, which may represent the predicted NF-κB or NFAT sites present within conserved sequence C (Fig. 2C). The calculated positions of the protected regions are shown at the very top of Fig. 5D, and these precisely match the positions of all of the previously defined and predicted clusters of transcription factor binding sites within the enhancer. Furthermore, the spacing between nuclease-hypersensitive sites within the enhancer N0/N1/N2 region in activated mast cells is only about 100 bp throughout this segment, which is incompatible with the coexistence of conventional phased nucleosomes within this 600-bp region. These observations suggest that the enhancer functions as distinct modules of mini-enhanceosomes, which essentially replace the nucleosomes within this region.

Nucleosomes are specifically positioned across at least 5 kb of the GM-CSF locus and are reorganized in activated cells. To confirm the above observations, DNase I and MNase cleavage sites were mapped in the same samples used in Fig. 5C from a PshA I site located 1.5 kb upstream of the enhancer (Fig. 6A and C). To further extend this analysis, the filter containing these samples was subsequently reprobed from a PshA I site 1.8 kb downstream of the transcription start site so as to examine sequences upstream of the enhancer and spanning the promoter (Fig. 6B and C). The analyses of relative MNase cleavage using the upstream probe revealed that nucleosomes were strictly phased and regularly positioned at ~200-bp intervals both within the enhancer and for at least 1 kb upstream of the enhancer in both T cells and mast cells (Fig. 6A and C). When combined with the analyses using the downstream probe, these data suggested that this regular 200-bp repeating pattern continued for at least 4 kb downstream of the enhancer in mast cells, indicating that at least 5 to 6 kb of the GM-CSF locus was occupied by a regular array of sequence-positioned nucleosomes. However, in T cells, this regular pattern of specific nucleosome positioning was less well defined than in mast cells for the regions just downstream of the enhancer and within the GM-CSF gene. There was also an indication that two alternate phases of nucleosome positions may overlap across a short transition region from approximately +600 to +900, where an additional series of MH bands (marked by asterisks in Fig. 6C) was present. Note that a 500-bp region midway between the two probes (−2000 to

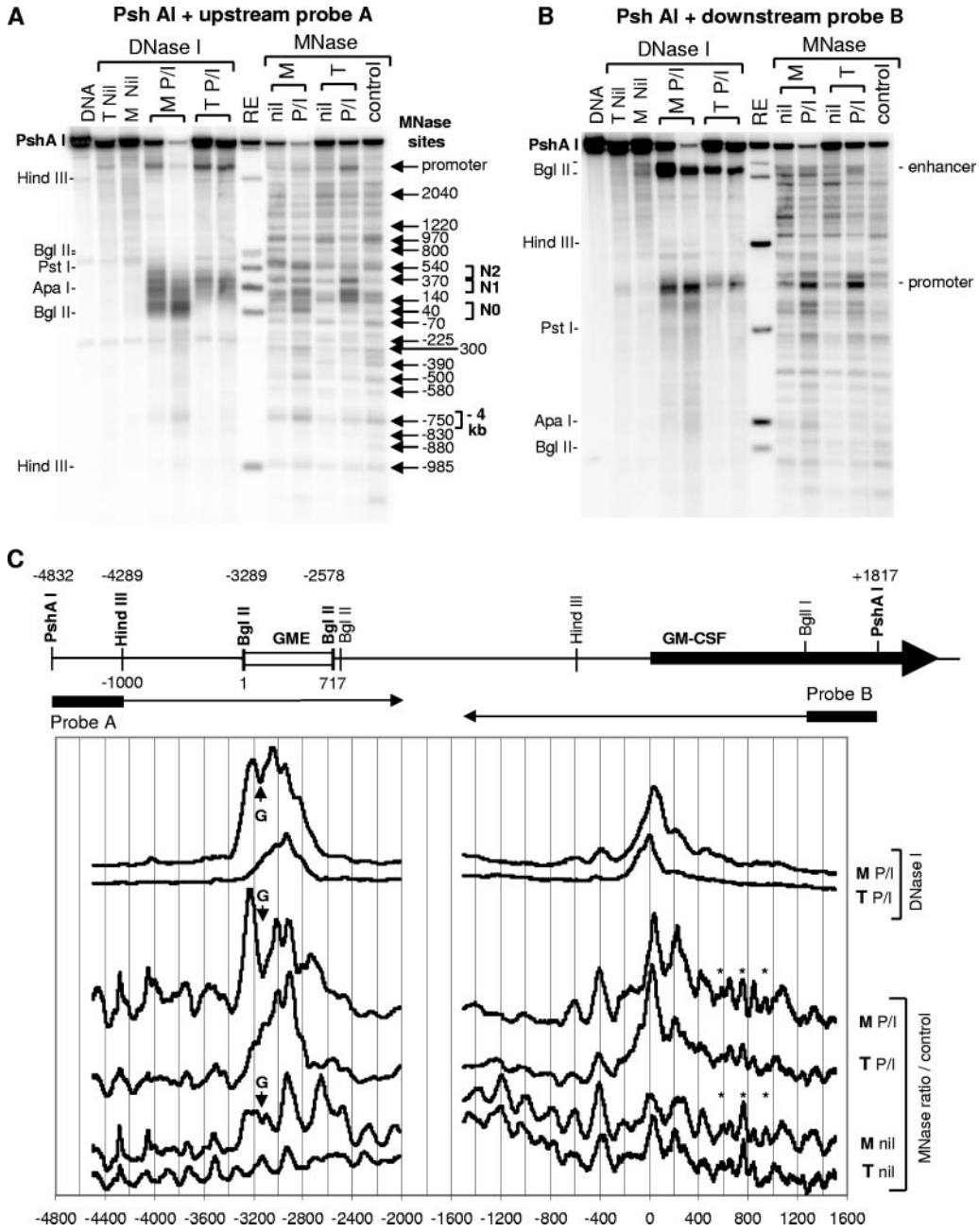

FIG. 6. Long-range nucleosomal organization and chromatin structure in the GM-CSF locus in mast cells and T cells. (A and B) Analyses of nuclease sensitivity within the GM-CSF enhancer using the same samples and methodology presented in Fig. 5C. These analyses employed upstream and downstream probes to detect cleavage sites relative to the PshAI sites as depicted in panel C. In panel A, the numbers to the right refer to positions relative to the GM-CSF enhancer 5′ BglII site. (C) Map of the GM-CSF locus depicting the PshAI sites and probes used to map cleavage sites in panels A and B. Numbers above the map indicate positions relative to the transcription start site, and numbers below indicate positions relative to the GM-CSF enhancer 5′ BglII site. The graphs below the map are as in Fig. 5D and represent the limits of mapping data obtained using either the upstream or downstream probes. The positions of the GATA sites are indicated by arrows labeled G. The asterisks indicate MNase sites that may reflect an alternate phasing of nucleosomes.

−1500) cannot be accurately mapped here due to the compression of bands within the upper part of each panel.

A strikingly different pattern of nucleosome organization was observed in activated T cells and mast cells. Here, the regular phasing of nucleosomes was largely randomized for both the sequences directly flanking the enhancer (Fig. 5D and 6C) and for much of the region between the enhancer and the promoter, but not for the far upstream sequences (Fig. 6C). Interestingly, nucleosomes flanking the promoter were maintained in strict positions after activation, and a region spanning the transcription start became strongly DNase I and MNase hypersensitive (Fig. 6C). The predicted nucleosomal linker

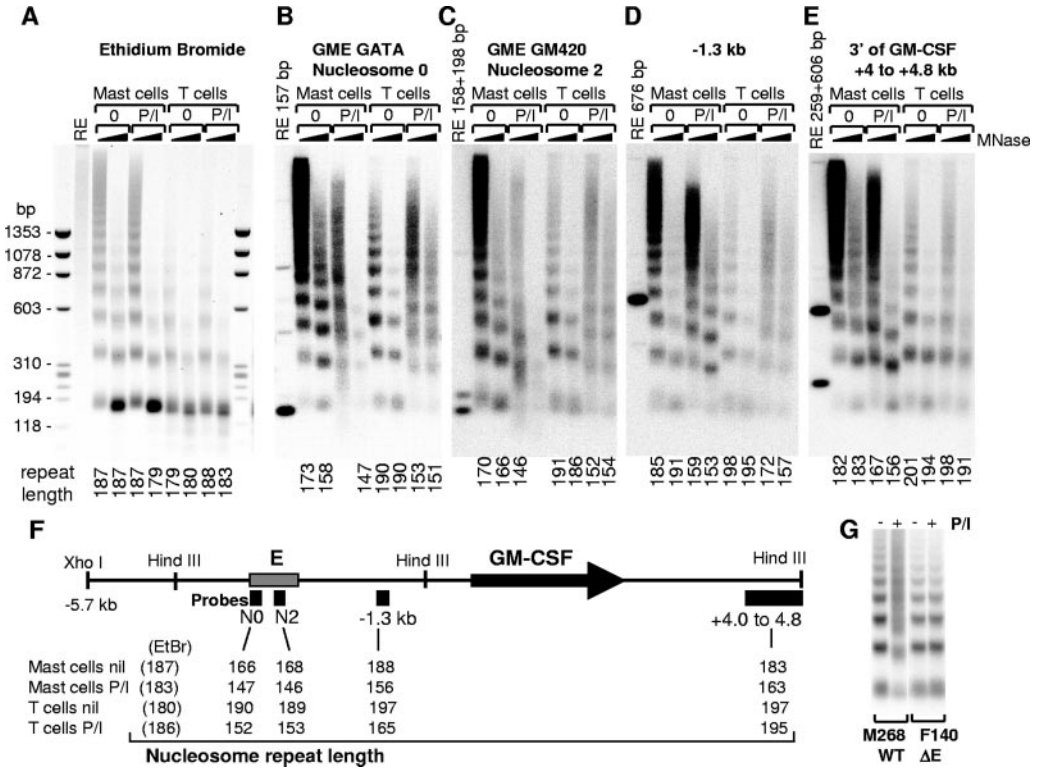

FIG. 7. Nucleosome destabilization and mobilization in the GM-CSF locus in mast cells and T cells. (A to F) Southern blot hybridization analysis of DNA purified from MNase-digested nuclei isolated from M268 GM-CSF transgenic mouse mast cells and T cells that were either unstimulated (0) or stimulated for 4 h with 20 ng/ml PMA and 2 μM A23187 (P/I). Each pair of MNase digestion conditions employed increasing concentrations of MNase digested within the range of 50 to 500 U/ml for 3 or 15 min using the probes depicted in panel F. (A) MNase digestion of bulk chromatin as detected by ethidium bromide staining, including the HaeIII ϕX174 marker used to determine sizes of oligonucleosome fragments. (B to E) Hybridization patterns obtained with the indicated probes. The left-hand lanes in each panel represent genomic DNA digested with PstI, ApaI, and BglII to produce fragments used to confirm appropriate hybridization specificity and validate quantification of size estimations. (F) Map of the GM-CSF transgene showing the locations of hybridization probes. Summarized below each probe are the average nucleosome repeat lengths determined from densitometry of the images in panels A to F. (G) MNase analyses of M268 and F140 transgenic T cells performed as described above, using 150 U/ml MNase for 15 min, and the −1.3-kb probe. F140 contains a transgene lacking the GM-CSF enhancer, as in Fig. 1A.

region at positions 200 to 250 was also hypersensitive in activated mast cells, with nucleosome-size protected regions remaining on either side. This suggests that two specifically positioned nucleosomes may remain between positions 0 and 400, but with the linkers more accessible in activated mast cells. Previous reports indicate that the nucleosome occupying the promoter is excluded in activated T cells (19, 21), and the presence of the broad peak of nuclease-sensitive peaks seen across the promoter here (Fig. 6C) is consistent with these findings.

The analyses of DNase I and MNase cleavage sites within the enhancer mapped from the upstream PshA I site (Fig. 6B and C) confirmed the observations presented in Fig. 5C. These studies similarly (i) revealed that nucleosomes occupy different positions within the enhancer in nonactivated T cells and mast cells (also summarized in Fig. 5E) and (ii) revealed the presence of DH and MH sites at ~100-bp intervals in activated cells, suggesting that nucleosomes are replaced by enhanceosome-like complexes. Once again, the DNase I and relative MNase cleavage patterns in activated cells were essentially identical and encompassed protected regions at the GM330 and GM420 elements in T cells and at both these sites and the GATA elements in mast cells (Fig. 6C). The analyses of nonactivated mast cells revealed the loss of nucleosome N0 and the clear presence of a short protected region corresponding to the GATA elements (marked by an arrow labeled G) (Fig. 5E and 6A and C). In this analysis, it is also evident that nucleosomes N1, N2, and N3 are maintained as specifically positioned nucleosomes within the enhancer in nonactivated mast cells but the linker regions flanking these nucleosomes are all hypersensitive to MNase relative to the flanking nucleosomes (Fig. 6C). These analyses also reveal a weak DH site present at −4 kb, corresponding to a myeloid-specific DH site (11).

Enhancer-dependent nucleosome mobilization in the GM-CSF locus. The above analyses suggested that nucleosomes were disrupted within the GM-CSF enhancer and disorganized across the sequences between the enhancer and promoter in both activated mast cells and T cells. To study nucleosome destabilization and mobilization more directly, we have employed internal nucleosome-length probes to determine whether nucleosomes are still present at specific locations and whether the surrounding nucleosome array is reorganized upon activation. Analyses of MNase-digested activated and nonactivated mast cells and T cells are shown in Fig. 7. Two

different MNase concentrations were used for each cell type, and samples were assayed (i) using three nucleosome-length probes corresponding to the T-cell positions for nucleosome N0, nucleosome N2, and a region midway between the enhancer and promoter (−1.3 kb); and (ii) with a 0.85-kb probe at the far 3′ end of the transgene (+4.0 to +4.8). The average nucleosome spacing in each lane was determined from the average band intervals by densitometry, using the DNA size marker as a reference, and is shown at the bottom of each lane (Fig. 7A to E). The average of each pair of lanes is presented in the summary in Fig. 7F. However, in these analyses, it is probably most useful to compare the most heavily digested mast cell samples with the equivalent least digested T-cell samples, because these show similar levels of cleavage of bulk DNA.

As in a previous study (21), we demonstrated that the GM-CSF locus existed as a regular nucleosome array in unstimulated T cells, with an average repeat length of ~190 to 200 bp. In unstimulated mast cells, the locus also existed as a regular array but the repeat length was reduced to about 166 to 168 bp in the vicinity of the enhancer and was ~10 bp shorter than in T cells in other regions. There was also significant loss of the enhancer N0 mononucleosome band, but not N2, in unstimulated mast cells but not in T cells (compare Fig. 7B and C).

Nucleosomes N0 and N2 were significantly disrupted in both activated T cells and mast cells. Furthermore, in activated T cells, nucleosomes were mobilized and randomized both across the enhancer and within the −1.3-kb region between the enhancer and the GM-CSF promoter. With the N0, N2 and −1.3-kb probes, the sharp banding pattern was lost in activated T cells and the faint remaining oligonucleosome bands had an average repeat length of just 150 to 165 bp, which is inconsistent with predicted models of a conventional 30-nm chromatin fiber (Fig. 7B to D).

Significantly, we also obtained evidence that the process of long-range nucleosome mobilization was enhancer dependent because no change in the chromatin structure of the −1.3-kb region was seen in activated T cells prepared from transgenic line F140, which lacks the GM-CSF enhancer (Fig. 7G). This indicates that the nucleosome mobilization seen upstream of the GM-CSF gene is a process that spreads from the enhancer, not the promoter.

In activated mast cells, disruption of N0 and N2 was also accompanied by randomization of the nucleosome array in this region and a decrease in the apparent nucleosome repeat length from ~167 to ~147 bp (Fig. 7B and C). Nucleosome mobilization across the GM-CSF locus was more extensive in mast cells than in T cells, with reduced nucleosome repeat lengths being detected at both the −1.3-kb region, and at the far 3′ end of the transgene (Fig. 7D and E). However, there was less randomization of nucleosome positions across the −1.3-kb region in activated mast cells than in T cells (Fig. 7D). In this instance, the banding patterns remained more sharply defined in mast cells, even though the repeat length in this region had decreased from 188 to 156 bp upon stimulation. This suggests that nucleosomes are uniformly closely packed at ~156-bp intervals in this region, but are not positioned at specific sequences as they are in nonstimulated mast cells (Fig. 6C). Taken together, these observations suggest that nucleosomes are excluded from the enhancer in activated mast cells and become compacted and randomized in the flanking sequences.

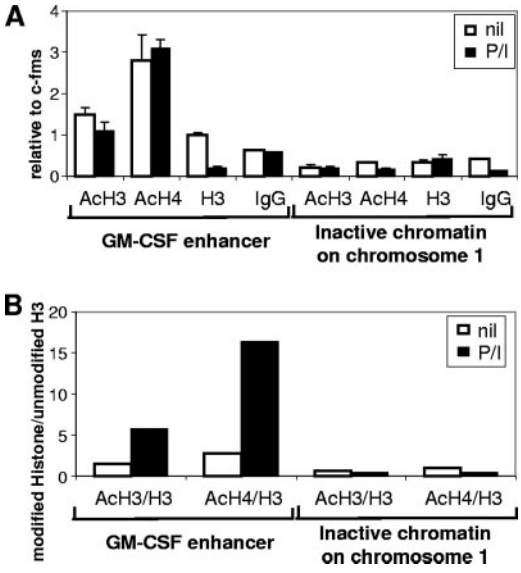

FIG. 8. ChIP assays of histones in mast cells. (A) Assays of acetyl K9 histone H3, pan-acetyl H4, unmodified histone H3, or control IgG, using real-time PCR primers located within the GM-CSF enhancer or an inactive control region on chromosome 1. Mast cells were prepared from line C42 transgenic mice and were either unstimulated (nil) or stimulated for 4 h with 20 ng/ml PMA and 2 μM A23187 (P/I). All values represent duplicate ChIP assays with error bars showing standard deviation and have been normalized to ChIP data obtained with the inactive c-*fms* locus. (B) Ratios of acetyl K9 H3 to unmodified H3 ChIP values.

GM-CSF enhancer nucleosomes are acetylated in mast cells. ChIP assays revealed that histones H3 and H4 were significantly acetylated within the enhancer relative to an inactive locus in both unstimulated and stimulated mast cells (Fig. 8A). The unmodified histone H3 assays also confirmed that nucleosomes were lost from the enhancer in stimulated mast cells (Fig. 8A), meaning that the relative level of histone acetylation was significantly elevated in stimulated mast cells (Fig. 8B). We found that these elevated levels of H3 and H4 acetylation extended from at least 7 kb upstream to at least 4.5 kb downstream of the GM-CSF gene, thereby encompassing the entire region of the locus where we observed nucleosome mobilization in mast cells (data not shown).

DISCUSSION

Modular organization and chromatin subdomains within the GM-CSF enhancer. Our data clearly show that the GM-CSF enhancer is modular and suggest that it forms a series of inducible tissue-specific enhanceosome-like complexes that replace nucleosomes. Furthermore, different modules, or even different elements within the modules, are utilized in different cell types. This is to our knowledge the first study to show a mechanism by which a single enhancer is divided into distinct modules that are differentially regulated and which adopts a different nucleosomal architecture in different cell types in which it is active. This type of regulation is different from other similar models, such as the IL-4 gene, which can be activated

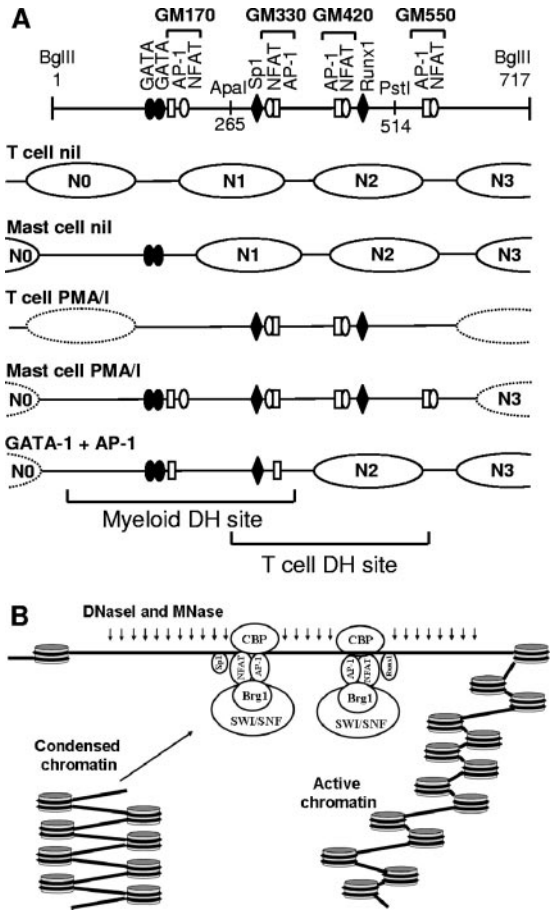

FIG. 9. Anatomy of a DH site. (A) Models of nucleosome reorganization and transcription factor recruitment in the GM-CSF enhancer. Each line below the map summarizes the predicted positions of nucleosomes and recruited transcription factors under different conditions. Large solid ovals represent specifically positioned nucleosomes. Dotted ovals indicate positions where nucleosomes adopt flexible positions. nil, unstimulated. (B) Scale model of enhanceosomes and nucleosomes within the activated GM-CSF enhancer in T cells.

by distinct well-separated enhancers in Th2 T cells and mast cells (24, 30). This pattern of regulation shares some similarity with the tumor necrosis factor alpha promoter, which assembles an Elk-1/CBP-dependent enhanceosome in response to LPS but distinct NFAT complexes across the same region in response to activation of Ca^{2+} signaling pathways (34).

As summarized in the model in Fig. 9A, two modules of the GM-CSF enhancer encompassing the GM330 and GM420 NFAT/AP-1 elements normally exist as nucleosomes N1 and N2. These modules can be defined as the GM330 element plus the adjacent Sp1 site on nucleosome N1 and the GM420 element plus the adjacent Runx1 site on nucleosome N2. In T cells, these regulatory elements are the only sites required for function and they also represent the only sites where we have detected in vivo footprints in activated T cells (21). In the previous study, NFAT was implicated as a factor that promoted nucleosome destabilization. Significantly, the earlier study found that an array of NFAT sites was sufficient to direct formation of an inducible DH site in Jurkat cells but was insufficient to activate transcription in the absence of AP-1 elements. Hence, at the GM-CSF enhancer, cooperation between NFAT and AP-1 appears to be obligatory in T cells, with NFAT directing a chromatin remodeling activity and AP-1 being recruited by NFAT and required for transcriptional activation. This model also accounts for the lack of in vivo footprints for the constitutively expressed factors Sp1 and Runx1 in unstimulated T cells, because these elements also reside within nucleosomes and thus depend on NFAT-dependent mechanisms for accessibility within chromatin.

The mechanism by which NFAT promotes nucleosome disruption remains unknown, but we have previously suggested that it may involve a SWI/SNF-like activity (9, 21). SWI/SNF is known to function by destabilizing nucleosomes (15) and is known to be recruited by the GM-CSF promoter (19). AP-1 is also known to bind to SWI/SNF (20), and NFAT and AP-1 each recruit CBP/P300 family proteins that may function in the context of the GM-CSF enhancer both as histone acetyl transferases and as scaffolding proteins in the assembly of enhanceosomes (1, 7, 17). We have, therefore, constructed a speculative model of what the DNase I HS site and the enhanceosomes may look like (Fig. 9B). In this scale model, it is apparent that the two enhanceosomes are likely to be much larger than the histone octamers they replace (~2,500 versus ~108 kDa), and the length of DNA that is released by the eviction of two nucleosomes is very broad in the context of the folded nucleosomes. The NFAT/AP-1 complexes alone constitute ~240 kDa. When viewed in this way, it begins to become apparent why DNase I HS sites are so much more accessible than folded chromatin fibers.

Regulation of the GM-CSF enhancer by GATA elements. In contrast to the pattern seen in T cells, the GATA region of the enhancer is governed very differently at the level of chromatin structure in myeloid cells. The presence of nuclear GATA-1 and GATA-2 in unstimulated mast cells appears to be sufficient to direct a pattern of nucleosome positioning very different from that seen in T cells. Unlike other elements in the enhancer, it is unlikely that GATA factors require significant chromatin remodeling to access the GATA elements because they lie within a broad ~60- to 75-bp nucleosome linker region. Furthermore, our previous restriction accessibility assays in T cells determined that this region is accessible to BamHI even in nonstimulated cells, whereas the ApaI and HincII sites just downstream are only accessible in activated cells (21). Our ChIP assays confirmed that GATA-2 binds to the enhancer in mast cells prior to activation. This event is likely to be responsible for promoting the acetylation of histones and the creation of an extensive nucleosome-free region that spans the normal position of nucleosome N0 and the entire conserved region stretching from the Ets-like element to the GM170 AP-1 element. This mode of regulation by GATA factors would also facilitate enhancer activation in myeloid cells lacking NFAT (such as K562 and HEL cells) where the enhancer functions efficiently in the absence of NFAT. As modeled in Fig. 9, the regulation of the enhancer in K562 and HEL cells by GATA-1 and AP-1 is associated with the formation of a discrete DH site spanning the GATA sites and the GM170 and GM330 AP-1 sites. In this context, activation is likely to lead to recruitment of AP-1 to the high-affinity GM170 and GM330 AP-1 elements and Sp1 to the GM300 element. We also have evidence that the GATA sites and the closely linked GM170 AP-1 site func-

tion as a discrete module because the GATA and GM170 sites are both needed for function in HMC-1 cells, whereas the GM330 and GM420 AP-1 sites are not (Fig. 3). It is also significant that GATA-2 and AP-1 have the capacity to directly associate with each other and are known to cooperate in the activation of the IL-13 promoter in mast cells (27). These observations, and the close proximity of the GATA and GM170 AP-1 sites, make it even more likely that this region of the GM-CSF enhancer functions as a discrete enhanceosome. GATA elements have also long been recognized as sites of tissue-specific chromatin remodeling, which is thought to be directed via SNF2H/ACF1 remodeling complexes recruited by GATA factors (32). This type of complex could also account for the repositioned nucleosomes that we observe in the GM-CSF enhancer because SNF2H is known to mediate nucleosome sliding (15).

Mechanisms of tissue-specific and high-level cytokine gene regulation. Our study also adds a new twist to the accepted models of the differential regulation of tissue-specific cytokine genes. In differentiated T cells, many cytokine genes are expressed in a mutually exclusive fashion by either Th2 or Th1 T-cell-specific mechanisms, whereas GM-CSF is expressed more widely. Th2-type cytokine genes, which include the IL-4, IL-5, and IL-13 genes, are all activated via NFAT and GATA-3 in Th2 T cells (13), and these genes are also coexpressed in mast cells. This makes it likely that the GATA and NFAT elements of the GM-CSF enhancer will also cooperate in Th2 T cells. This means that the GM-CSF enhancer may be activated by Th2-type mechanisms in Th2 cells, mast cells, and eosinophils, but by quite distinct mechanisms in other cells such as Th1 T cells and nonhemopoietic cells. It is also apparent that the recruitment of GATA factors leads to very high levels of GM-CSF locus activation. Mast cells which express GATA, NFAT, and AP-1 factors expressed $\sim 10^4$-fold-higher levels of GM-CSF than CD11b-positive splenocytes (Fig. 1C) and fetal liver-derived macrophages (E. W. Baxter and P. N. Cockerill, unpublished data), which both express NFAT and AP-1 but not GATA factors. The enhancer was also considerably more active in transfection assays of myeloid cells expressing GATA factors than in Jurkat T cells, which do not (Fig. 4). Furthermore, it is likely that the IL-4-dependent activation of GATA-3 gene expression will synergize with T-cell receptor signaling pathways to drive higher levels of GM-CSF expression in Th2 T cells than in undifferentiated T cells.

Enhancer-dependent nucleosome mobilization in the GM-CSF locus. Surprisingly few previous studies have looked at long-range nucleosome mobilization or found alterations in nucleosome repeat length at active gene loci in mammalian cells. We have made the highly significant observation that activation of an enhancer can lead to dramatic changes in the structure of the whole chromatin fiber across several kilobases of DNA. In both T cells and mast cells, activation of the enhancer led to a reduction in local nucleosome repeat length from a normal value of about 190 bp in nonactivated T cells to about 153 bp in activated T cells and 146 bp in activated mast cells. This reduced value is essentially the same as the size of the 146-bp nucleosome core particle and is significantly shorter than the 167 bp required to assemble a chromatosome comprising the core plus histone H1. With essentially no significant nucleosomal linkers, it is difficult to see how this structure could form any kind of folded chromatin fiber that might resemble the 30-nm fiber.

Chromatin reorganization in the active GM-CSF locus was not restricted to the immediate vicinity of the enhancer, but continued more than a kilobase into the −1.3-kb region, where the nucleosome repeat lengths were 165 in activated T cells and 156 in activated mast cells. In activated mast cells, inducible histone acetylation and nucleosome reorganization also extended at least 2 kb past the 3′ end of the GM-CSF gene where nucleosome repeat lengths were still about 20 bp less than those in nonactivated cells. Significantly, we also demonstrated that nucleosome mobilization upstream of the GM-CSF promoter was dependent upon the enhancer, suggesting that this may represent a significant component of the mechanism of enhancer function.

Nucleosome mobilization leads to randomization. When attempting to interpret our data, it is important to acknowledge that the predominant pattern of nucleosome mobilization in the GM-CSF locus (Fig. 6 and 7) is actually randomization of nucleosome positioning rather than simply shortening of nucleosome repeat lengths. In activated T cells, the discrete nucleosomal fragments seen after MNase digestion of mobilized regions (Fig. 7) do in fact only represent a small proportion of the total products, which mostly appear as a continuous spectrum of sizes. The small proportion of discrete products emanating from the activated GM-CSF locus most likely arise by a stochastic process whereby a subset of nucleosomes will inevitably lie in closely packed positions within an essentially random organization. In the case of the −1.3-kb region in activated mast cells, it would appear that a higher proportion of nucleosomes become more tightly packed and generate a more uniform nucleosome ladder (Fig. 7D), without adopting new specific positions (Fig. 6C). We have attempted to represent models of the regular array and the mobilized array in Fig. 9B.

Other examples of nucleosome mobilization at active genes. There are currently very few known examples of any other gene loci where gene activation is accompanied by a reduction in apparent nucleosome repeat length. One of the only mammalian examples is the active mouse kappa Ig gene locus, which has a calculated repeat length of 155 bp in B cells compared to 175 bp for an inactive globin gene (36). Other nonmammalian examples are the *Chlamydomonas HSP70A* and *RBCS2* loci, with repeat lengths of 160 and 156 bp compared to 178 bp in bulk chromatin (26), and an inducible yeast *GAL1* promoter construct which undergoes a repeat length decrease from 180 to 160 bp upon activation (6). The simplest explanation for the observed compaction of nucleosomes in the active GM-CSF locus is the exclusion of nucleosomes from the enhancer, accompanied by the loss of histone H1 from the adjacent sequences. Histone H1 depletion in mice is known to decrease the global nucleosome repeat length (16). Furthermore, there is a precedent for gene locus activation leading to a reduction of H1 levels, not only at *cis*-regulatory elements, but also within flanking regions (25).

There are also other similar previous examples of active gene loci undergoing extensive randomization of nucleosome organization (6, 12, 22, 23, 36), although in one such study of the β-globin locus (22), there was no parallel decrease in nucleosome repeat length. In one of the yeast studies mentioned above, nucleosome mobilization was dependent upon SWI/

SNF (23), and we and others have previously suggested that a Brg1-dependent SWI/SNF-like mechanism may underlie nucleosome disruption and mobilization at the GM-CSF locus (9, 19, 21). Another mechanism likely to be involved in nucleosome mobilization is the acetylation of histone H4 at lysine 16, which is known to be sufficient to induce unfolding of the 30-nm chromatin fiber (33). It is therefore also significant that we detect acetylation of histones H3 and H4 at the GM-CSF enhancer. We anticipate that long-range nucleosome reorganization occurs more commonly in active genes than is currently recognized and represents a fundamental aspect of gene activation that is likely to involve a variety of chromatin modifications acting together to create an active chromatin structure.

ACKNOWLEDGMENTS

We thank D. Roberts, D. Brooke, A. Horner, and L. Williams for creating and managing the transgenic mice; F. Ponchel for advice on real-time PCR assays; G. Doody for help with fluorescence-activated cell sorting assays; and P. Lefevre for advice on ChIP assays. We thank J. Gamble for providing endothelial cells and C. Bonifer for her input and advice on mast cells and for assistance revising the manuscript. We also thank M. F. Shannon and M. A. Vadas for their input and support.

This work was supported by Yorkshire Cancer Research, the AICR, and the NH&MRC.

REFERENCES

1. **Avots, A., M. Buttmann, S. Chuvpilo, C. Escher, U. Smola, A. J. Bannister, U. R. Rapp, T. Kouzarides, and E. Serfling.** 1999. CBP/p300 integrates Raf/Rac-signaling pathways in the transcriptional induction of NF-ATc during T cell activation. Immunity **10:**515–524.
2. **Baxter, E. W., W. J. Cummings, and R. E. Fournier.** 2005. Formation of a large, complex domain of histone hyperacetylation at human 14q32.1 requires the serpin locus control region. Nucleic Acids Res. **33:**3313–3322.
3. **Bert, A. G., J. Burrows, A. Hawwari, M. A. Vadas, and P. N. Cockerill.** 2000. Reconstitution of T cell-specific transcription directed by composite NFAT/Oct elements. J. Immunol. **165:**5646–5655.
4. **Butterfield, J. H., and D. A. Weiler.** 1989. In vitro sensitivity of immature human mast cells to chemotherapeutic agents. Int. Arch. Allergy Appl. Immunol. **89:**297–300.
5. **Carey, M.** 1998. The enhanceosome and transcriptional synergy. Cell **92:**5–8.
6. **Cavalli, G., and F. Thoma.** 1993. Chromatin transitions during activation and repression of galactose-regulated genes in yeast. EMBO J. **12:**4603–4613.
7. **Chan, H. M., and N. B. La Thangue.** 2001. p300/CBP proteins: HATs for transcriptional bridges and scaffolds. J. Cell Sci. **114:**2363–2373.
8. **Chen, L.** 1999. Combinatorial gene regulation by eukaryotic transcription factors. Curr. Opin. Struct. Biol. **9:**48–55.
9. **Cockerill, P. N.** 2004. Mechanisms of transcriptional regulation of the human IL-3/GM-CSF locus by inducible tissue-specific promoters and enhancers. Crit. Rev. Immunol. **24:**385–408.
10. **Cockerill, P. N., A. G. Bert, F. Jenkins, G. R. Ryan, M. F. Shannon, and M. A. Vadas.** 1995. Human granulocyte-macrophage colony-stimulating factor enhancer function is associated with cooperative interactions between AP-1 and NFATp/c. Mol. Cell. Biol. **15:**2071–2079.
11. **Cockerill, P. N., A. G. Bert, D. Roberts, and M. A. Vadas.** 1999. The human GM-CSF gene is autonomously regulated in vivo by an inducible tissue-specific enhancer. Proc. Natl. Acad. Sci. USA **96:**15097–15102.
12. **Cohen, R. B., and M. Sheffery.** 1985. Nucleosome disruption precedes transcription and is largely limited to the transcribed domain of globin genes in murine erythroleukemia cells. J. Mol. Biol. **182:**109–129.
13. **Dong, C., and R. A. Flavell.** 2001. Th1 and Th2 cells. Curr. Opin. Hematol. **8:**47–51.
14. **Drew, E., H. Merkens, S. Chelliah, R. Doyonnas, and K. M. McNagny.** 2002. CD34 is a specific marker of mature murine mast cells. Exp. Hematol. **30:**1211.
15. **Fan, H. Y., X. He, R. E. Kingston, and G. J. Narlikar.** 2003. Distinct strategies to make nucleosomal DNA accessible. Mol. Cell **11:**1311–1322.
16. **Fan, Y., T. Nikitina, J. Zhao, T. J. Fleury, R. Bhattacharyya, E. E. Bouhassira, A. Stein, C. L. Woodcock, and A. I. Skoultchi.** 2005. Histone H1 depletion in mammals alters global chromatin structure but causes specific changes in gene regulation. Cell **123:**1199–1212.
17. **Garcia-Rodriguez, C., and A. Rao.** 1998. Nuclear factor of activated T cells (NFAT)-dependent transactivation regulated by the coactivators p300/CREB-binding protein (CBP). J. Exp. Med. **187:**2031–2036.
18. **Hawwari, A., J. Burrows, M. A. Vadas, and P. N. Cockerill.** 2002. The human IL-3 locus is regulated cooperatively by two NFAT-dependent enhancers that have distinct tissue-specific activities. J. Immunol. **169:**1876–1886.
19. **Holloway, A. F., S. Rao, X. Chen, and M. F. Shannon.** 2003. Changes in chromatin accessibility across the GM-CSF promoter upon T cell activation are dependent on nuclear factor kappaB proteins. J. Exp. Med. **197:**413–423.
20. **Ito, T., M. Yamauchi, M. Nishina, N. Yamamichi, T. Mizutani, M. Ui, M. Murakami, and H. Iba.** 2001. Identification of SWI.SNF complex subunit BAF60a as a determinant of the transactivation potential of Fos/Jun dimers. J. Biol. Chem. **276:**2852–2857.
21. **Johnson, B. V., A. G. Bert, G. R. Ryan, A. Condina, and P. N. Cockerill.** 2004. Granulocyte-macrophage colony-stimulating factor enhancer activation requires cooperation between NFAT and AP-1 elements and is associated with extensive nucleosome reorganization. Mol. Cell. Biol. **24:**7914–7930.
22. **Kim, A., and A. Dean.** 2003. A human globin enhancer causes both discrete and widespread alterations in chromatin structure. Mol. Cell. Biol. **23:**8099–8109.
23. **Kim, Y., N. McLaughlin, K. Lindstrom, T. Tsukiyama, and D. J. Clark.** 2006. Activation of *Saccharomyces cerevisiae HIS3* results in Gcn4p-dependent, SWI/SNF-dependent mobilization of nucleosomes over the entire gene. Mol. Cell. Biol. **26:**8607–8622.
24. **Kwan, M., D. R. Powell, T. Y. Nachman, and M. A. Brown.** 2005. An intron GATA-binding site regulates chromatin accessibility and is essential for IL-4 gene expression in mast cells. Eur. J. Immunol. **35:**1267–1274.
25. **Lefevre, P., C. Lacroix, H. Tagoh, M. Hoogenkamp, S. Melnik, R. Ingram, and C. Bonifer.** 2005. Differentiation-dependent alterations in histone methylation and chromatin architecture at the inducible chicken lysozyme gene. J. Biol. Chem. **280:**27552–27560.
26. **Lodha, M., and M. Schroda.** 2005. Analysis of chromatin structure in the control regions of the chlamydomonas HSP70A and RBCS2 genes. Plant Mol. Biol. **59:**501–513.
27. **Masuda, A., Y. Yoshikai, H. Kume, and T. Matsuguchi.** 2004. The interaction between GATA proteins and activator protein-1 promotes the transcription of IL-13 in mast cells. J. Immunol. **173:**5564–5573.
28. **Merika, M., and D. Thanos.** 2001. Enhanceosomes. Curr. Opin. Genet. Dev. **11:**205–208.
29. **Merika, M., A. J. Williams, G. Chen, T. Collins, and D. Thanos.** 1998. Recruitment of CBP/p300 by the IFN beta enhanceosome is required for synergistic activation of transcription. Mol. Cell **1:**277–287.
30. **Monticelli, S., D. U. Lee, J. Nardone, D. L. Bolton, and A. Rao.** 2005. Chromatin-based regulation of cytokine transcription in Th2 cells and mast cells. Int. Immunol. **17:**1513–1524.
31. **Orkin, S. H.** 1995. Hematopoiesis: how does it happen? Curr. Opin. Cell Biol. **7:**870–877.
32. **Rodriguez, P., E. Bonte, J. Krijgsveld, K. E. Kolodziej, B. Guyot, A. J. Heck, P. Vyas, E. de Boer, F. Grosveld, and J. Strouboulis.** 2005. GATA-1 forms distinct activating and repressive complexes in erythroid cells. EMBO J. **24:**2354–2366.
33. **Shogren-Knaak, M., H. Ishii, J. M. Sun, M. J. Pazin, J. R. Davie, and C. L. Peterson.** 2006. Histone H4-K16 acetylation controls chromatin structure and protein interactions. Science **311:**844–847.
34. **Tsai, E. Y., J. V. Falvo, A. V. Tsytsykova, A. K. Barczak, A. M. Reimold, L. H. Glimcher, M. J. Fenton, D. C. Gordon, I. F. Dunn, and A. E. Goldfeld.** 2000. A lipopolysaccharide-specific enhancer complex involving Ets, Elk-1, Sp1, and CREB binding protein and p300 is recruited to the tumor necrosis factor alpha promoter in vivo. Mol. Cell. Biol. **20:**6084–6094.
35. **Walsh, J. C., R. P. DeKoter, H. J. Lee, E. D. Smith, D. W. Lancki, M. F. Gurish, D. S. Friend, R. L. Stevens, J. Anastasi, and H. Singh.** 2002. Cooperative and antagonistic interplay between PU.1 and GATA-2 in the specification of myeloid cell fates. Immunity **17:**665–676.
36. **Xu, M., M. B. Barnard, S. M. Rose, P. N. Cockerill, S. Y. Huang, and W. T. Garrard.** 1986. Transcription termination and chromatin structure of the active immunoglobulin kappa gene locus. J. Biol. Chem. **261:**3838–3845.